Biophysical Chemistry 199 (2015) 1–8

Contents lists available at ScienceDirect

Biophysical Chemistry

journal homepage: http://www.elsevier.com/locate/biophyschem

# Relationship between structural composition and material properties of polymorphic hIAPP fibrils

Myeongsang Lee [a], Hyun Joon Chang [a], Donghoi Kim [c], Yongwoo Lee [c], Heesu Suh [c], Namjo Ahn [c], Gwonchan Yoon [a,b,*], Sungsoo Na [a,**]

[a] Department of Mechanical Engineering Korea University, Seoul 136-701, Republic of Korea
[b] Department of Mechanical Engineering, Boston University, Boston, MA 02115, USA
[c] Seoul Science High School, Seoul 110-530, Republic of Korea

## HIGHLIGHTS

- This study shows the structural characteristic of polymorphic hIAPP fibrils via constant force steered molecular dynamics simulations.
- Stacking direction and arrangement of beta strands affects the elastic modulus of hIAPP fibrils.
- The antiparallel model is found to have a higher elastic modulus compared to that of the parallel model.

## GRAPHICAL ABSTRACT

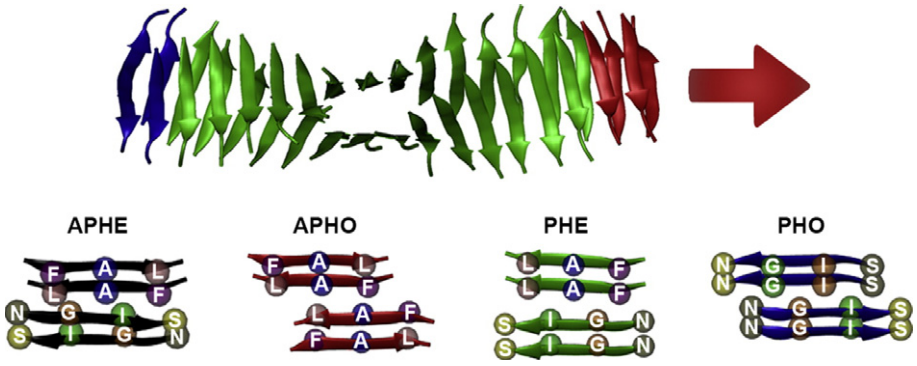


## ARTICLE INFO

*Article history:*
Received 5 December 2014
Received in revised form 14 January 2015
Accepted 2 February 2015
Available online 7 February 2015

*Keywords:*
hIAPP fibrils
Steered molecular dynamics
Polymorphic structures

## ABSTRACT

Amyloid proteins are misfolded, denatured proteins that are responsible for causing several degenerative and neuro-degenerative diseases. Determining the mechanical stability of these amyloids is crucial for understanding the disease mechanisms, which will guide us in treatment. Furthermore, many research groups recognized amyloid proteins as functional biological materials that can be used in nanosensors, bacterial biofilms, coatings, etc. Many in vitro studies have been carried out to determine the characteristics of amyloid proteins via force spectroscopy methods, atomic force microscopy, and optical tweezers. However, computational methods (e.g. molecular dynamics and elastic network model) not only reveal the mechanical properties of the amyloid proteins, but also provide more in-depth information about the amyloids by presenting a visualization of their conformational changes. In this study, we evaluated the various material properties and behaviors of four different polymorphic structures of human islet amyloid polypeptide (hIAPP) by using steered molecular dynamics (SMD) simulations under tensile conditions. From our results, we examined how these mechanical properties may differ with respect to the structural formation of amyloid proteins.



## 1. Introduction

Pathological amyloid diseases are associated with several degenerative and neuro-degenerative diseases, such as senile heart disease, type II diabetes, Alzheimer's disease, and Huntington's disease [1,2]. The

* Correspondence to: G. Yoon, Department of Mechanical Engineering, Boston University, Boston, MA 02115, USA.
** Correspondence to: S. Na, Department of Mechanical Engineering, Korea University, Seoul 136-713, Republic of Korea.
*E-mail addresses:* gyoon1@bu.edu (G. Yoon), nass@korea.ac.kr (S. Na).

http://dx.doi.org/10.1016/j.bpc.2015.02.002
0301-4622/

origins of these diseases are the amyloid proteins developed by denatured and misfolded proteins [3,4], which disrupt and reduce the normal function of cells or proteins in the human body. Amyloid proteins such as tau, HET-s, human islet amyloid polypeptides (hIAPP), Aβ, β2-microglobulin, and β2-lactoglobulin fibrils exhibit various forms, such as 1D structures (i.e. nanotube and fibrillar structures) and 2D structures (i.e. films and angled layer structures) with hierarchical compositions of β strands [5]. The existence of amyloid fibrils in these forms can be referred to as polymorphism along with the various compositions and directions of β strands [6–8]. Furthermore, the thickness variation of amyloid fibrils as well as the number of protofibril structure were observed [9]. These amyloid proteins share cross β structures sustained with steric zipper interaction that renders them difficult to degrade in physiological environments [10–13]. Thus, understanding the stability of amyloid proteins has been recognized as a crucial step in elucidating the mechanisms of degenerative and neuro-degenerative diseases and providing treatment for these diseases.

However, the focus of research on amyloid fibrils has shifted from the role of the fibrils as a source of pathological diseases to their use as functional biological materials for conductive materials, nanosensors, bacterial biofilms, and coatings [14–16]. Amyloid proteins themselves possess material stability and mechanical properties, which can be compared to nanomaterials and biological materials, which could be evaluated by using force spectroscopy methods (i.e. atomic force microscopy and optical tweezers) and computational methods (i.e. molecular dynamics simulation and elastic network model) [17]. Knowles et al. demonstrated the material properties and characteristics of various kinds of amyloid fibrils such as insulin, TTR (105–115) (transthyretin), β-lactoglobulin and α-lactalbumin via experimental and computation methods, for example, reaching up to ~10 GPa of elastic moduli [18]. The study revealed that the cause of different structures of amyloid fibrils is the varying numbers of hydrogen bonds, and the material properties and characteristics may also vary depending on the cross section of area. Buehler et al. predicted the elastic modulus and rigidity of amyloid fibrils via various computational methods [19]. For these reasons, the role of amyloid fibrils has been risen in their use as a template for functional materials.

Many research groups have already developed amyloid fibril templates for functional materials such as nanosensors and nanodevices. For instance, in terms of amyloid nanosensors, Li et al. developed a selective gas sensor at given environments using amyloid fibrils [20]. They used tau amyloid protein as the selective capturing tool for carbon dioxide under various ranges of temperature and pressure. For amyloid fibrils used as conductive materials, Scheibel et al. developed amyloid fibrils as a template for conductive materials using gold nanoparticles [21]. In a similar manner, Li et al. developed functional conductive materials with shape-memory characteristics using α-lactoglobulin amyloid fibrils with graphene nanosheets [22]. From their study, they sustained excellent conductive characteristics with advanced material properties by adding amyloid fibrils. Yolamanova et al. utilized amyloid fibrils as enhancers of retroviral transduction to increase gene transfer in mice models [23]. Furthermore, Perutz et al. suggested that specific sequences of amyloid fibrils could form water-filled nanotubes [24].

From the various functional studies concerning amyloid materials, amyloid fibrils have been developed and used as functional materials due to their excellent material properties such as high elastic moduli, bending rigidity and toughness. Therefore, understanding the properties and characteristics of amyloid fibrils is important for the development of functional material templates using amyloid materials with various characteristics. Buehler et al. revealed, using tensile loading simulations via the number of hydrogen bonds broken, that the wide range of material properties exhibited by amyloid fibrils, such as two stacked β-sheets fibrils, three β-helical fibrils, and mixed fibrils, depended on the cross-sectional area [25]. Yoon et al. examined the differences in the structural and mechanical properties of HET-s fibrils comparing left-handed and right-handed directions using NMA (normal mode analysis) simulations [26]. They also found that the material responses and properties were related to the secondary structure composition of amyloid fibrils. Ndlovu et al. studied the material response of wild-type and mutated hIAPP fibrils using various types of SMD (steered molecular dynamics) simulations [27]. From their study, they found the role of the hydrophobic residues and the effect of mutation on the stability of hIAPP fibrils. In this regard, the study of amyloid as a template for functional materials in terms of their material properties and characteristics is needed.

In our previous studies, we showed the material properties and characteristics of polymorphic hIAPP fibrils, which were evaluated via different types of deformation modes such as soft bending, stiff bending, torsion, and axial, using eigenvalue problems with ENM (elastic network model) and MD simulations [28,29]. Moreover, recently we studied the different material behaviors of hIAPP fibrils using constant bending simulations [30,31]. From our study, we showed the brittleness and ductility of polymorphic hIAPP fibrils as well as their material properties, such as Young's modulus and fracture toughness. Recently, Ndlvou et al. revealed the mechanical responses of four types of polymorphic hIAPP fibrils using different modes of SMD simulations [32]. They addressed that the mechanical responses of polymorphic hIAPP fibrils depended on structural composition. However, it is still challenging for the material property characterization of hIAPP fibrils using tensile loading simulations.

In the current study, we examined the material characteristics of the four kinds of polymorphic hIAPP fibrils using tensile SMD simulations. We observed that the elastic properties in the diverse polymorphs of hIAPP fibrils depended on the parallel and antiparallel structural composition or homo and hetero structural composition. Moreover, we determined the fracture toughness values using the number of broken hydrogen bonds and revealed the material characteristics of hIAPP fibrils.

## 2. Material and methods

### 2.1. Construction of polymorphic hIAPP structures

Amyloid proteins, such as Aβ, tau, prions, and insulin, have polymorphic characteristics because of their different structures, orientation with respect to the β strands, and their parallel or antiparallel compositions, as reported by Sawaya et al. [6]. The hIAPP amyloid proteins used in this study had eight kinds of polymorphic characteristics depending on the orientation of the stacked β strands (i.e. parallel and antiparallel), facing sides of β strands (i.e. homo and hetero), and direction of β strands themselves (i.e. co-aligned and anti-aligned), as shown by Neilson et al. [8]. To investigate the relationship between structural compositions based on the organization of each β strand, we considered four basic kinds of polymorphic structures: antiparallel hetero (APHE), antiparallel homo (APHO), parallel hetero (PHE) and parallel homo (PHO) (see Fig. 1(a), (b), (c) and (d) respectively). To construct the computational models of the polymorphic hIAPP structures, we adopted information from the PDB (Protein Data Bank), where the protein has an ID of 2KIB. The sequence used in this study is NFGAILS from the full sequences of hIAPP fibrils. Based on existing geometric information, we stacked the cross β strands, which are 8.75 nm in length scale, 4.7 Å along the axis direction [33]. During the stacking process of the hIAPP structure, we stacked the polymorphic structures sustained with steric zipper interaction to avoid penetration of water molecules between facing two cross β strands. In this process, the intersheet interaction was sustained as dry interfaces and no water molecules between facing β strands were found, also shown in Esposito et al. [10].

### 2.2. Composing polymorphic hIAPP fibrils

To form helical fibrillar shape of hIAPP fibrils from the stacked structures, we conducted equilibrated simulation on the polymorphic hIAPP

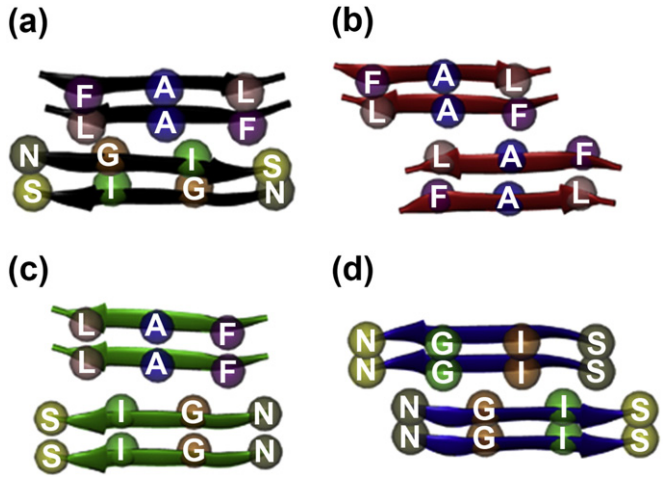


**Fig. 1.** The schematic view of polymorphic structures of hIAPP building blocks. The four residues such as F, A, L and I are hydrophobic residues which play an important role to sustain the stability of the hIAPP fibrils. (a) APHE model of hIAPP. (b) APHO model of hIAPP. (c) PHE model of hIAPP. (d) PHO model of hIAPP.

structure. We applied the NAMD 2.7b with a CHARMM 27 force field under explicit solvent conditions using a TIP3P model [34]. For the construction of explicit solvent condition, we applied the 20 Å size of water padding. An NVT ensemble was applied during equilibrated simulation at 300 K. Before equilibration simulations, conjugate gradient methods were applied 10,000 times. During the equilibrated MD simulation, all bond length was constrained. In addition, short range for VDW interaction was calculated using switching function distance between 10 Å and 12 Å. Thereafter, 10 ns equilibration simulation proceeded at 2 fs per step. After equilibration of MD simulation, the stacked hIAPP structure converged to helical fibrillar shapes with average 15° of dihedral angle. For analysis, equilibrated simulation was elapsed for 10 ns for each model and resulting trajectory was saved every 3 ps. No structural changes were observed after 5 ns of equilibrium simulations.

### 2.3. Material characterization of polymorphic hIAPP fibrils

After 10 ns equilibration simulations, we obtained four stable configurations of hIAPP fibrils from each polymorphic hAIPP fibril. To determine the stability and material characteristics of the four kinds of hIAPP fibrils, we applied SMD simulations. We applied fix-free conditions for each type of hIAPP fibril with a constant velocity loading condition of 0.01 Å/ps and a spring constant of 500 pN/Å (Fig. 2). The 1st and 2nd layers of hIAPP fibrils were fixed and the 17th and 18th layers of hIAPP fibrils were selected for loading constraints. The remaining atoms were allowed to move freely during SMD simulations. SMD simulations were elapsed for 5 ns for each hIAPP fibril and trajectories were saved every 3 ps. Same as equilibrated MD simulation process, we used the NAMD 2.7b package with a CHARMM27 force field condition during SMD simulation.

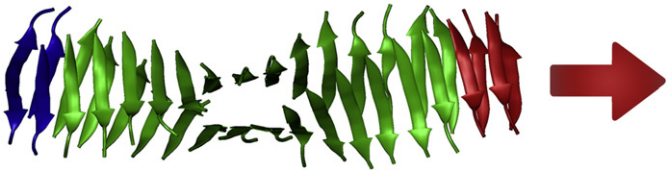

**Fig. 2.** Constraint schematic of hIAPP fibrils for fix-free constraint tensile loading simulation. Blue color means the fixed area and red area color means the pulled area.

### 2.4. Analysis of material characteristics of polymorphic hIAPP fibrils

Analysis of SMD simulations was performed on each loading trajectory based on the results of SMD simulations via VMD (visual molecular dynamics) for each polymorphic hIAPP fibril [35]. During the SMD simulations, the atomic position and force of hIAPP fibril were obtained with respect to time step. For the sake of analysis, first 2 ns MD simulation was considered, while remaining 3 ns trajectories of each model were retained as fractured. To characterize the material response of hIAPP fibrils, fracture toughness ($\Upsilon$) was calculated using the following equation:

$$\Upsilon = \frac{F_p \times \delta_F}{V}. \quad (1)$$

Here, $F_p$ represents the peak force value when hIAPP fibril was fractured during the loading simulations, $\delta_F$ is the fractured displacement value when adjacent β strands were separated during the loading simulations, and $V$ is the volume of polymorphic hIAPP fibrils, which reached up to $1.5 \times 10^{-26}$ $m^3$. To reveal the material properties of polymorphic hIAPP fibrils via loading simulations, we rearranged the time–force relationship between strain–stress relationships using Hooke's law:

$$\sigma = E\varepsilon. \quad (2)$$

Herein, $\sigma$ is the stress of tensile loading applied on the cross-section of hIAPP fibril structures which is obtained from relationship between the force and the cross section area. $E$ is the Young's modulus, and $\varepsilon$ is the strain from the reference length of hIAPP fibrils. To obtain the strain, the following equation was applied at

$$\varepsilon = \frac{L(i+1) - L(1)}{L(1)}. \quad (3)$$

Here, $L(i+1)$ is the changed length of hIAPP fibril and $L(1)$ is the initial length of hIAPP fibril. To support the material characteristics and properties of hIAPP fibrils, we measured the non-bonded energy and the number of hydrogen bonds using NAMD energy and hydrogen bond plugins of VMD. In order to investigate the fractured H-bonds of polymorphic hIAPP fibrillar structure, we selected the fractured H-bond areas which composed of inter-strand H-bonds around the fracture layers. After that, we calculated the fractured H-bonds through following relationship:

$$\Delta H_{fracted} = H(1) - H(1 + i). \quad (4)$$

Here, $H(1)$ is the number of hydrogen bond of initial structure, and $H(i+1)$ is the number of H-bonds when structure of hIAPP fibrillar changed along time step.

## 3. Results

In this study, we examined the material characteristics of polymorphic hIAPP fibrils through constant velocity tensile loading simulations. From the simulation results, we addressed the polymorphic behavior of polymorphic hIAPP fibrils and the role of hydrophobic amino acids via the peak force responses of hIAPP fibrils. Furthermore, we also observed mechanical properties and plastic material behaviors of hIAPP fibrils through their Young's modulus and fracture toughness.

### 3.1. Different mechanical responses of polymorphic hIAPP fibrils

Before analyzing the structural characteristic of polymorphic hIAPP amyloid fibrils, the structural modeling results of hIAPP fibrils was to be compared with previous studies [28,30]. We revealed that the similarity of structural configuration of hIAPP fibrils and the rupture number

of hydrogen bonds obtained by the present study were compared to those earlier studies. Through the constant velocity loading simulations, we obtained the mechanical responses of polymorphic hIAPP fibrils depending on their orientation with respect to β strands and stacking directions. We found that the results of time–force curves and trajectory changes reflect the polymorphic behavior of hIAPP fibrils. We marked the fracture trajectory of polymorphic hIAPP fibril as the $T_0$, $T_1$, $T_2$ and $T_3$ of Fig. 3, which was determined by distinct fracture events, and these marked events show similar consistency with time–force curves of Fig 3(e), (f), (g) and (h). From Fig 3, we found similar molecular deformation through the constant velocity loading simulations for each model, even though the mechanical responses were different for each other. The homo model showed a higher peak force value than that of hetero model, including antiparallel and parallel models for each as seen in Fig. 3. However, we observed that the antiparallel models, which were composed of AHPO and APHE, had higher peak force at time sections near 0.1 ns than the parallel models (PHO and PHE) did near 0.2 ns. Although the peak force responses of the homo model were higher than the hetero model, including the antiparallel model, the material behavior is different.

### 3.2. Material characteristics of polymorphic hIAPP fibrils

In addition to time–force curves, we studied the different material behaviors of polymorphic hIAPP fibrils via strain–stress curves resulting from Hooke's law which is shown in Fig. 4 using the number of

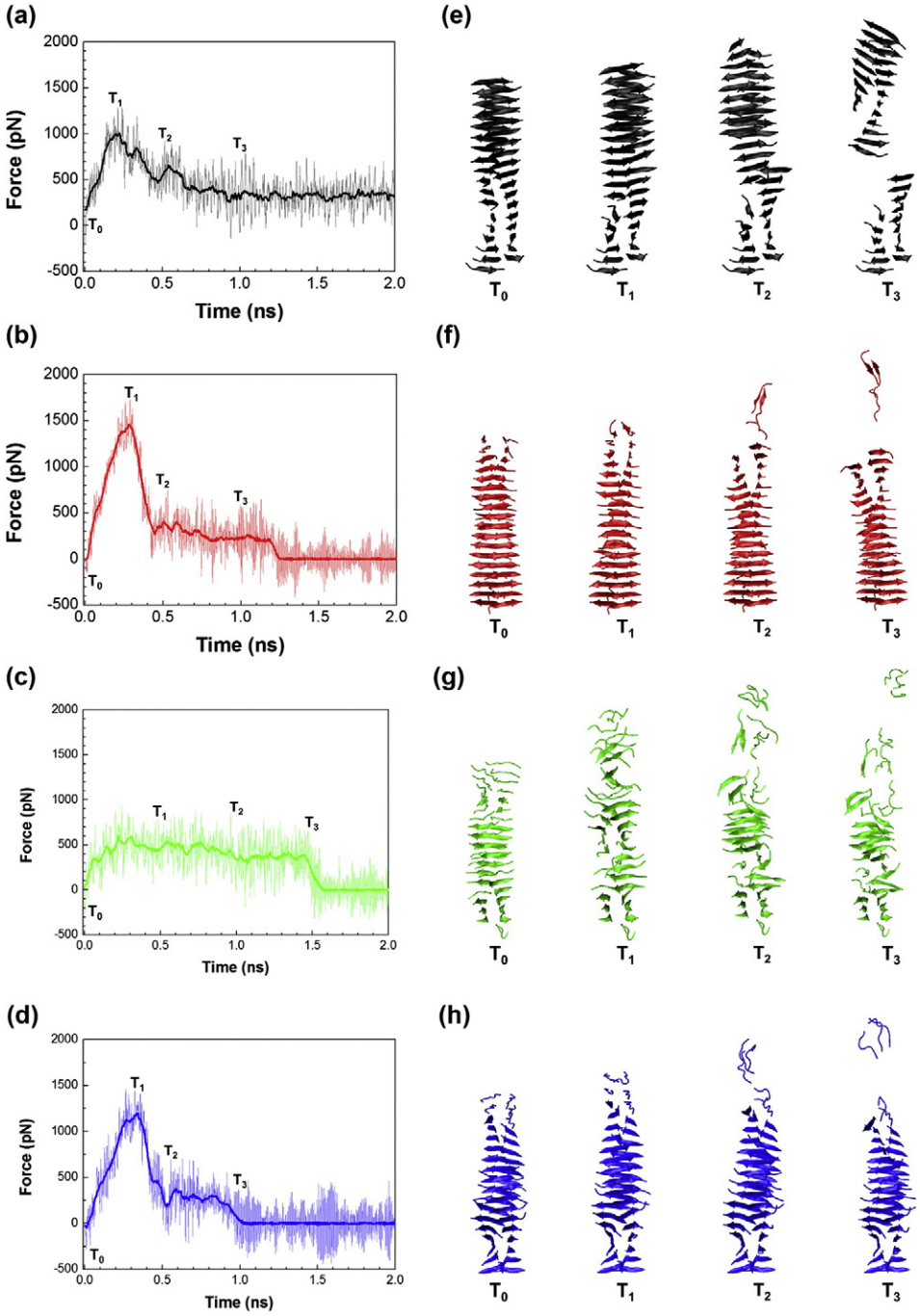


**Fig. 3.** The time–force curves and fracture process of 4 kinds of polymorphic hIAPP fibrils. (a) APHE model of hIAPP. (b) APHO model of hIAPP. (c) PHE model of hIAPP. (d) PHO model of hIAPP. Fracture process trajectory models for (e), (f), (g) and (h) are same as time–force graphs.

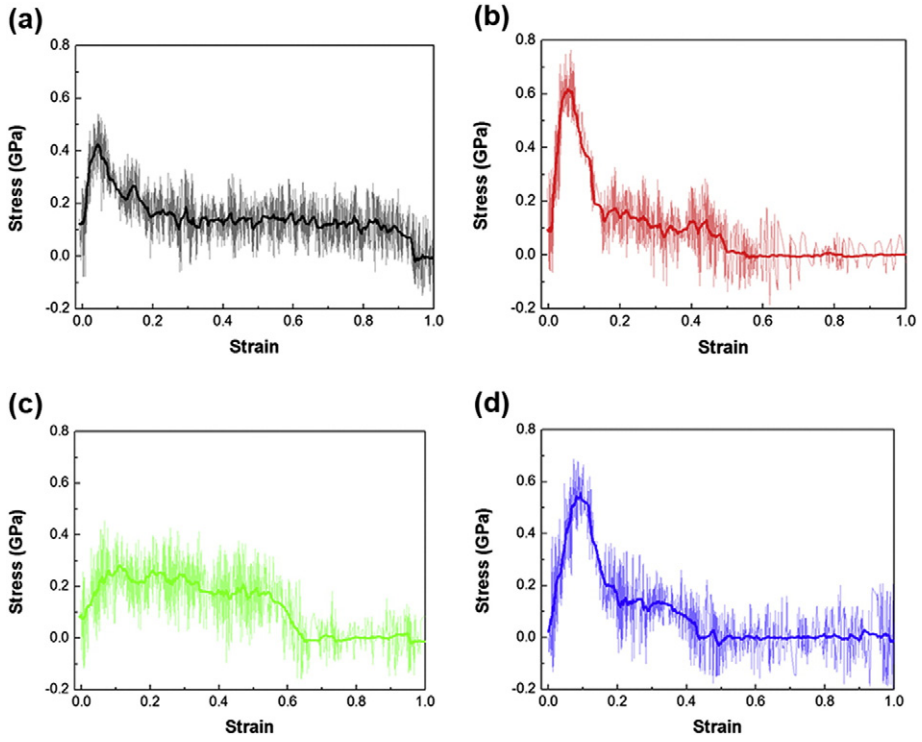


**Fig. 4.** The strain–stress curves of 4 kinds of polymorphic hIAPP fibrils. (a) APHE model of hIAPP. (b) APHO model of hIAPP. (c) PHE model of hIAPP. (d) PHO model of hIAPP.

hydrogen bonds and the location of hydrophobic amino acids. We calculated the Young's modulus through the slop of initial linear increasing region in the stress–strain curve as shown in Fig. 4. We found, from the results of Young's modulus, that all polymorphic hIAPP fibrils exhibited elastic characteristics, as shown in Fig. 5, which show 9.82, 11.62, 2.55, and 5.97 GPa for APHE, APHO, PHE, and PHO, respectively. Also, we addressed the role of hydrogen bonds, shown in Fig 6, from the difference in tensile elastic modulus between the antiparallel and parallel models. Furthermore, the role of hydrophobic amino acids could be presented through the differences between the homo and hetero models, including parallel and antiparallel models. In contrast to time–force curves, material responses would be different and reflected the previous study, which revealed the polymorphic characteristics of hIAPP fibrils by solving eigenvalue problems [29].

### 3.3. Mechanical properties of hIAPP fibrils

With time–force and strain–stress curves, we found the mechanical properties of polymorphic hIAPP fibrils via their elastic modulus and fracture toughness. With time–force curves, we displayed the peak force response of polymorphic for each hIAPP fibrils, which could be compared with other measured methods such as peel, slide, and shear applied on similar wild-type and mutated hIAPP fibrils. Also, from the results of strain–stress curves, we found stress response of hIAPP compared with other biological materials, such as Aβ, HET-s, and collagen fibrils in spite of the differences in cross-sectional area [25]. Our results showed similar tendencies compared with experimental data, which confirmed the outstanding mechanical properties of insulin amyloid fibrils via AFM experiments [36]. Based on the plastic behavior of hIAPP fibrils during the constant velocity loading simulations, fracture toughness can be calculated. The fracture toughness for 4 kinds of polymorphic hIAPP fibrils can be calculated with Eq. (1), which is 20–60 MJ/m$^3$. Considering spider silk, a source of bullet-proof vests, has toughness values even under a high degree of applied force with 91 MJ/m$^3$ [39], our model shows high fracture toughness values for each polymorphic model.

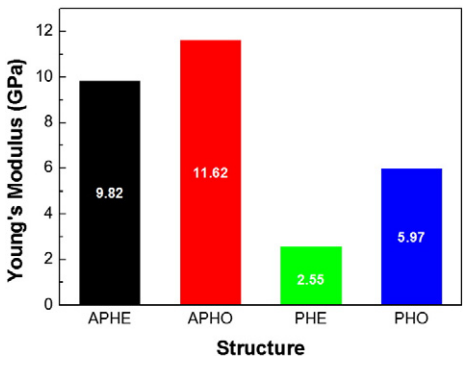


**Fig. 5.** Young's modulus value graphs for 4 kinds of polymorphic hIAPP fibrils.

## 4. Discussions

### 4.1. Location of hydrophobic amino acids affects the stability of polymorphic hIAPP fibrils

Ndlovu et al. studied the mechanical responses of polymorphic hIAPP fibrils using various loading modes [32], and Max et al. and Xu et al. found the reactions of different types of amyloid fibrils based on their cross-sectional area, demonstrating their mechanical response and stability using SMD (steered molecular dynamics) and NMA (normal model analysis) simulations [25,37]. From our present study, we also examined the various mechanical responses of polymorphic hIAPP using time–force curves in spite of similar rupture trajectory of each polymorphic hIAPP fibril. In Fig. 3(a) and (b), the antiparallel model takes longer time to reach peak forces than the parallel model does shown in Fig. 3(c) and (d). And we found that the peak force of the homo models (i.e. APHO and PHO) exhibited higher peak force values than those of hetero models (i.e. APHE and PHE) considering the structural composition characteristic which classified as face to face (homo) and face to back (hetero) composition. These tendencies were caused by the location of hydrophobic amino acid residues used

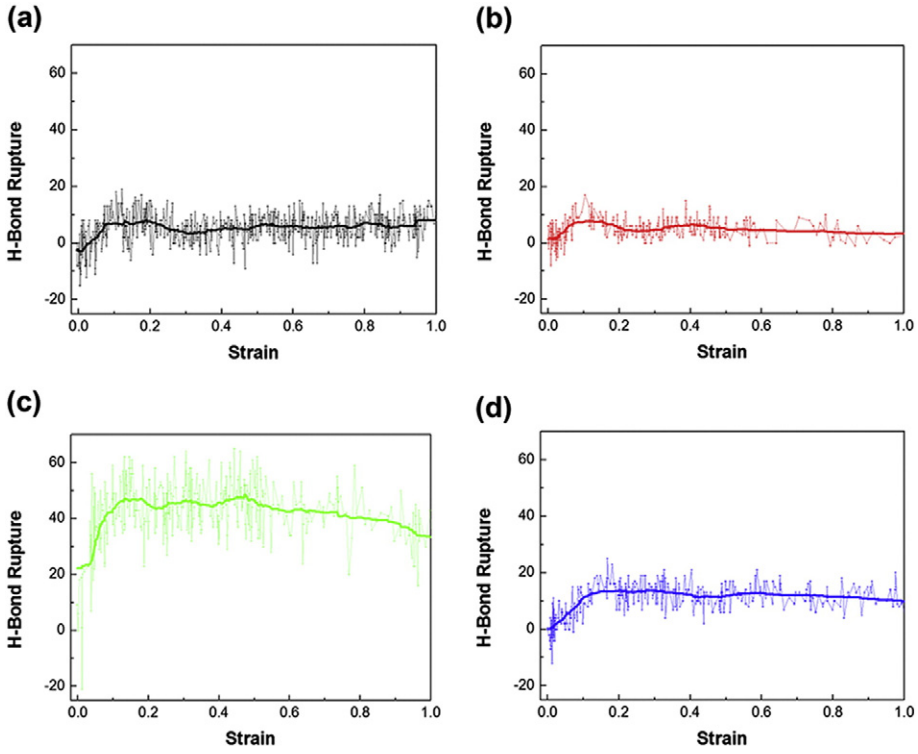


**Fig. 6.** Fracture number of hydrogen bonds versus strain graph. (a) APHE model of hIAPP. (b) APHO model of hIAPP. (c) PHE model of hIAPP. (d) PHO model of hIAPP.

in this study, which were A (alanine), F (phenylalanine), I (isoleucine), and L (leucine). Specifically, the PHO model had hydrophobic amino acids (F, A, and L) on the outside of the hIAPP fibrils. However, in the PHE model, only one hydrophobic amino acid was found on the outside of the hIAPP fibrils with less resistance to water structures compared with the PHO model. Our previous studies revealed the polymorphic characteristics of the PHO and PHE models using constant force and velocity bending simulations [30]. From present studies, the PHO model showed larger enduring times before force peak than the PHE model via time–force and displacement–force curves in Fig. 3, meaning that the PHO model was more stable than the PHE model. These tendencies also can be found in fracture process during the SMD simulations. From the fracture trajectories, we revealed the similar fracture location of APHO and PHO models. Also, despite the unstable conformation of PHE model, APHE and PHE models show the similar fracture location. These tendencies are caused by the characteristic of homo and hetero structure composition. The locations of hydrophobic amino acids affected the elastic modulus values, as shown in Table 1. From the table, the homo models, including parallel and antiparallel, show higher elastic moduli value than the hetero models. These results can be compared with our previous study, which determined the elastic modulus through eigenvalue analysis using MD and ENM analysis [28,29]. Despite having different loading methods in this study, we demonstrated similar tendencies between the PHO and PHE models via constant force loading simulations. Therefore, the role of the hydrophobic amino acids could be found through the constant force tensile loading simulations.

### *4.2. The role of hydrogen bonds in the stability of polymorphic hIAPP fibrils*

Our previous study reported the role of hydrogen bonds between parallel and antiparallel structures using eigenvalue problems [29]. We found that antiparallel models, including homo and hetero models, had better material properties than the parallel models. In this study, we evaluated the role of hydrogen bonds in the material characteristics of polymorphic hIAPP fibrils via constant velocity tensile loading simulations. In Figs. 5 and 6, we remark the effects of hydrogen bonding between the antiparallel and parallel models. The tensile elastic modulus of the antiparallel models (i.e. APHO and APHE) is larger than that of the parallel models (i.e. PHO and PHE). These tendencies are supported by the number of broken hydrogen bonds as shown in Fig. 6. The parallel models have a larger number of broken hydrogen bonds than the antiparallel models, which implies a lower stability in the parallel models. On the other hand, the antiparallel models show fewer broken hydrogen bonds compared with the parallel models. Also, the number of broken hydrogen bonds, assessed based on strain, shows similar tendencies, which implies that the properties of amyloid proteins depend on the cross-sectional area (i.e. HET-s, type II diabetes, and Aβ) [25]. The stability and properties of the antiparallel models are shown to be better than the parallel models through the tensile elastic modulus and the number of broken hydrogen bonds. These tendencies also can be shown in our previous data obtained by solving eigenvalue problems, whereby the antiparallel models show better material properties than the parallel models [29]. These structural characteristics depend on the stacking direction (i.e. antiparallel and parallel) and are similar to

**Table 1**
The tensile Young's modulus of 4 kinds of polymorphic hIAPP nanowire compared with other fibrils obtained by experimental and simulation methods.

| Model (methods) | hIAPP (our method) | hIAPP (ENM) [29] | Insulin (AFM experiment) [36] | Spider silk (experiment) [41] | Aβ (AFM experiment, MD) [18,25,38] |
|---|---|---|---|---|---|
| Young's moduli (GPa) | 2.4–12 | 12–14 | 3.3 ± 0.4 | 16–28 | 12.4–17.2 |

those reported in the study of Ndlovu et al., which examined the mechanical response of polymorphic hIAPP fibrils using various loading modes [32]. Thus, the role of hydrogen bonds and their effects on the stability and characteristics of polymorphic hIAPP fibrils depend on the stacking directions (i.e. antiparallel and parallel).

### 4.3. Elastic properties and plastic behavior of hIAPP fibrils

Normally, biological materials such as spider silk, amyloid proteins, and collagen, which possess outstanding material properties, are mainly composed of native contacts with hydrogen bonds [18], which possess remarkable bending rigidity and elastic modulus. In this study, we reported the tensile elastic modulus of polymorphic hIAPP models approached up to ~12 GPa, which can be compared to the results obtained from various loading modes, such as soft and stiff bending [30]. Also, our elastic modulus of polymorphic hIAPP fibrils can be compared to similar biological material such as Aβ amyloid fibrils which show compressive and tensile elastic modulus reaches up to ~18 GPa. In spite of the various methods applied on similar biological materials, the elastic modulus was similar due to native contacts such as hydrogen bonding and non-bonded energies [38]. Because of their remarkable elastic modulus and characteristics, amyloid fibrils are known as elastic materials and possess not only elastic characteristics, but also excellent toughness. We also found prominent fracture toughness values for each polymorphic hIAPP model. These results can be compared with our previous results, which applied constant force and velocity according to different bending directions [30,31]. Furthermore, the results can also be compared with spider silk, which is mainly composed of rich β strands with various crystal areas [39,40]. Although different loading conditions have been applied in this study to compare our results to previous studies, we observed the similar fracture toughness of polymorphic hIAPP fibrils.

## 5. Conclusions

In this study, we addressed the various material behaviors of polymorphic hIAPP fibrils via constant velocity tensile loading MD simulations. All polymorphic models exhibited remarkable elastic modulus and fracture toughness values, which could be compared with other biological materials. Based on the location of hydrophobic amino acids such as leucine, isoleucine, alanine, and phenylalanine, each polymorphic model showed different material characteristics. In particular, the antiparallel models, APHO and APHE, showed higher elastic modulus and fracture toughness values than those of parallel models via analysis of the number of broken hydrogen bonds. This study sheds light on the use of amyloids as a template for functional biological materials.

## Acknowledgment

S.N. gratefully acknowledges the Basic Science Research Program through the National Research Foundation of Korea (NRF) funded by the Ministry of Science, ICT & Future Planning (MSIP) (No. 2007-0056094). G.Y. is grateful for the financial support from the NRF under Grant No. 2012R1A1A2038373 and Korea University Grant. H.J.C. is grateful for the financial support from the Global PH.D Fellowship Program through the National Research Foundation of Korea (NRF), funded by the Ministry of Education (No. 2014H1A2A1021042).

## References

[1] M.B. Pepys, Amyloidosis, Annu. Rev. Med. 57 (2006) 223–241.
[2] D. Eisenberg, M. Jucker, The amyloid state of proteins in human diseases, Cell 148 (2012) 1188–1203.
[3] G. Merlini, V. Bellotti, Molecular mechanisms of amyloidosis, N. Engl. J. Med. 349 (2003) 583–596.
[4] C. Soto, Unfolding the role of protein misfolding in neurodegenerative diseases, Nat. Rev. Neurosci. 4 (2003) 49–60.
[5] N. Mizuno, U. Baxa, A.C. Steven, Structural dependence of HET-s amyloid fibril infectivity assessed by cryoelectron microscopy, Proc. Natl. Acad. Sci. U. S. A. 108 (2011) 3252–3257.
[6] M.R. Sawaya, S. Sambashivan, R. Nelson, M.I. Ivanova, S.A. Sievers, M.I. Apostol, et al., Atomic structures of amyloid cross-[bgr] spines reveal varied steric zippers, Nature 447 (2007) 453–457.
[7] Y. Miller, B. Ma, R. Nussinov, Polymorphism in Alzheimer Aβ amyloid organization reflects conformational selection in a rugged energy landscape, Chem. Rev. 110 (2010) 4820–4838.
[8] J.T. Nielsen, M. Bjerring, M.D. Jeppesen, R.O. Pedersen, J.M. Pedersen, K.L. Hein, et al., Unique identification of supramolecular structures in amyloid fibrils by solid-state NMR spectroscopy, Angew. Chem. 121 (2009) 2152–2155.
[9] J. Adamcik, J.-M. Jung, J. Flakowski, Rios P. De Los, G. Dietler, R. Mezzenga, Understanding amyloid aggregation by statistical analysis of atomic force microscopy images, Nat. Nanotechnol. 5 (2010) 423–428.
[10] L. Esposito, C. Pedone, L. Vitagliano, Molecular dynamics analyses of cross-β-spine steric zipper models: β-Sheet twisting and aggregation, Proc. Natl. Acad. Sci. U. S. A. 103 (2006) 11533–11538.
[11] B.-H. Kim, N.Y. Palermo, Sn. Lovas, T. Zaikova, J.F.W. Keana, Y.L. Lyubchenko, Single-molecule atomic force microscopy force spectroscopy study of Aβ-40 interactions, Biochemistry 50 (2011) 5154–5162.
[12] F. Hane, G. Tran, S.J. Attwood, Z. Leonenko, $Cu^{2+}$ affects amyloid-β (1–42) aggregation by increasing peptide-peptide binding forces, PLoS One 8 (2013) e59005.
[13] Y. Miller, B. Ma, C.-J. Tsai, R. Nussinov, Hollow core of Alzheimer's Aβ42 amyloid observed by cryoEM is relevant at physiological pH, Proc. Natl. Acad. Sci. U. S. A. 107 (2010) 14128–14133.
[14] T.P.J. Knowles, M.J. Buehler, Nanomechanics of functional and pathological amyloid materials, Nat. Nanotechnol. 6 (2011) 469–479.
[15] I. Cherny, E. Gazit, Amyloids: not only pathological agents but also ordered nanomaterials, Angew. Chem. Int. Ed. 47 (2008) 4062–4069.
[16] C.A.E. Hauser, S. Maurer-Stroh, I.C. Martins, Amyloid-based nanosensors and nanodevices, Chem. Soc. Rev. 43 (2014) 5326–5345.
[17] K.C. Neuman, A. Nagy, Single-molecule force spectroscopy: optical tweezers, magnetic tweezers and atomic force microscopy, Nat. Methods 5 (2008) 491–505.
[18] T.P. Knowles, A.W. Fitzpatrick, S. Meehan, H.R. Mott, M. Vendruscolo, C.M. Dobson, et al., Role of intermolecular forces in defining material properties of protein nanofibrils, Science 318 (2007) 1900–1903.
[19] M.J. Buehler, Y.C. Yung, Deformation and failure of protein materials in physiologically extreme conditions and disease, Nat. Mater. 8 (2009) 175–188.
[20] D. Li, H. Furukawa, H. Deng, C. Liu, O.M. Yaghi, D.S. Eisenberg, Designed amyloid fibers as materials for selective carbon dioxide capture, Proc. Natl. Acad. Sci. U. S. A. 111 (2014) 191–196.
[21] T. Scheibel, R. Parthasarathy, G. Sawicki, X.-M. Lin, H. Jaeger, S.L. Lindquist, Conducting nanowires built by controlled self-assembly of amyloid fibers and selective metal deposition, Proc. Natl. Acad. Sci. U. S. A. 100 (2003) 4527–4532.
[22] C. Li, J. Adamcik, R. Mezzenga, Biodegradable nanocomposites of amyloid fibrils and graphene with shape-memory and enzyme-sensing properties, Nat. Nanotechnol. 7 (2012) 421–427.
[23] M. Yolamanova, C. Meier, A.K. Shaytan, V. Vas, C.W. Bertoncini, F. Arnold, et al., Peptide nanofibrils boost retroviral gene transfer and provide a rapid means for concentrating viruses, Nat. Nanotechnol. 8 (2013) 130–136.
[24] M.F. Perutz, J.T. Finch, J. Berriman, A. Lesk, Amyloid fibers are water-filled nanotubes, Proc. Natl. Acad. Sci. U. S. A. 99 (2002) 5591–5595.
[25] S. Max, J.B. Markus, Tensile deformation and failure of amyloid and amyloid-like protein fibrils, Nanotechnology 25 (2014) 105703.
[26] G. Yoon, Y. Kab Kim, K. Eom, S. Na, Relationship between disease-specific structures of amyloid fibrils and their mechanical properties, Appl. Phys. Lett. (2013) 102.
[27] H. Ndlovu, E. Ashcroft Alison, E. Radford Sheena, Sarah A. Harris, Effect of sequence variation on the mechanical response of amyloid fibrils probed by steered molecular dynamics simulation, Biophys. J. 102 (2012) 587–596.
[28] G. Yoon, M. Lee, J.I. Kim, S. Na, K. Eom, Role of sequence and structural polymorphism on the mechanical properties of amyloid fibrils, PLoS One 9 (2014) e88502.
[29] G. Yoon, J. Kwak, J.I. Kim, S. Na, K. Eom, Mechanical characterization of amyloid fibrils using coarse-grained normal mode analysis, Adv. Funct. Mater. 21 (2011) 3454–3463.
[30] M. Lee, I. Baek, H.J. Chang, G. Yoon, S. Na, The bond survival time variation of polymorphic amyloid fibrils in the mechanical insight, Chem. Phys. Lett. 600 (2014) 68–72.
[31] J.I. Kim, M. Lee, I. Baek, G. Yoon, S. Na, The mechanical response of hIAPP nanowires based on different bending direction simulations, Phys. Chem. Chem. Phys. 16 (2014) 18493–18500.
[32] H. Ndlovu, A.E. Ashcroft, S.E. Radford, S.A. Harris, Molecular dynamics simulations of mechanical failure in polymorphic arrangements of amyloid fibrils containing structural defects, Beilstein J. Nanotechnol. 4 (2013) 429–440.
[33] J. Madine, E. Jack, P.G. Stockley, S.E. Radford, L.C. Serpell, D.A. Middleton, Structural insights into the polymorphism of amyloid-like fibrils formed by region 20–29 of amylin revealed by solid-state NMR and X-ray fiber diffraction, J. Am. Chem. Soc. 130 (2008) 14990–15001.
[34] J.C. Phillips, R. Braun, W. Wang, J. Gumbart, E. Tajkhorshid, E. Villa, et al., Scalable molecular dynamics with NAMD, J. Comput. Chem. 26 (2005) 1781–1802.
[35] W. Humphrey, A. Dalke, K. Schulten, VMD: visual molecular dynamics, J. Mol. Graph. 14 (1996) 33–38.
[36] J.F. Smith, T.P.J. Knowles, C.M. Dobson, C.E. MacPhee, M.E. Welland, Characterization of the nanoscale properties of individual amyloid fibrils, Proc. Natl. Acad. Sci. U. S. A. 103 (2006) 15806–15811.

[37] Z. Xu, R. Paparcone, M.J. Buehler, Alzheimer's Aβ(1–40) amyloid fibrils feature size-dependent mechanical properties, Biophys. J. 98 (2010) 2053–2062.
[38] R. Paparcone, S. Keten, M.J. Buehler, Atomistic simulation of nanomechanical properties of Alzheimer's Aβ(1–40) amyloid fibrils under compressive and tensile loading, J. Biomech. 43 (2010) 1196–1201.
[39] J.M. Gosline, P.A. Guerette, C.S. Ortlepp, K.N. Savage, The mechanical design of spider silks: from fibroin sequence to mechanical function, J. Exp. Biol. 202 (1999) 3295–3303.
[40] A. Nova, S. Keten, N.M. Pugno, A. Redaelli, M.J. Buehler, Molecular and nanostructural mechanisms of deformation, strength and toughness of spider silk fibrils, Nano Lett. 10 (2010) 2626–2634.
[41] P.M. Cunniff, S.A. Fossey, M.A. Auerbach, J.W. Song, D.L. Kaplan, W.W. Adams, R.K. Eby, D. Mahoney, D.L. Vezie, Mechanical and thermal properties of dragline silk from the spider *Nephila clavipes*, Polym. Adv. Technol. 5 (1994) 401–410.